Progress in Superconductivity and Cryogenics
Vol.15, No.2, (2013), pp.39~43 http://dx.doi.org/10.9714/psac.2013.15.2.039

Evaluation of Mg size dependence on superconductivity of MgB_2

B. B. Sinha[a], S. H. Jang[a], K. C. Chung[*, a], J. H. Kim[b], and S. X. Dou[b]

[a] *Korea Institute of Material Science, Changwon, Korea*
[b] *Institute for Superconducting and Electronic Materials, Univ. of Wollongong, Australia*

(Received 8 June 2013; revised or reviewed 21 June 2013; accepted 22 June 2013)

Abstract:

MgB_2 bulk samples are synthesized through solid state reaction route using Mg precursors with different particle size by keeping the boron precursor unchanged. Scanning electron microscopy study of the fractured surface for all the samples depicts quite distinct structure depending on the Mg precursor. Big size of Mg precursor resulted in to largely elongated and deep pores while smaller one gave roughly ellipsoidal and shallow pore structure. Influence of the Mg particle size on the grain to grain connectivity reflected in the critical current density value which was greater for samples with smaller Mg precursor. All the synthesized samples undergo a superconducting transition at around 36.5 K irrespective of different Mg precursor particle size.

Keywords : Superconductivity, Magnesium diboride, Critical current density

1. INTRODUCTION

Unlike the low temperature Nb-based superconductor, MgB_2 has a higher superconducting transition temperature of 39K [1] even though it has a simple binary crystal structure like A15 superconductors. Further it does not need significant texturing due to its weak-link-free intergrain connectivity that lacks in HTS superconductors [2-4]. Thus it has quite remarkable advantages over HTS compounds, but lags behind in the crucial parameter of infield critical current density. It has been found that chemically [5-7] or physically [8] altering the interband scattering can drastically enhance the MgB_2 superconducting properties such as upper critical field, irreversibility field etc., which in-turn enhance the critical current density. High critical current density values are seen in case of MgB_2 thin films [9], this provide us hints for possibility of achieving the necessary superconducting properties that will make MgB_2 strong on the grounds of practical applications. The present investigation is dedicated to the study of enhancement in the superconducting property of the bulk MgB_2 samples as an effect of different sized Mg precursor.

2. EXPERIMENTAL

MgB_2 samples were prepared by conventional solid state reaction method. Here different size of Mg precursor powder about 99.9% pure and boron powder with 95-97% purity was used. Five different size of Mg precursor was prepared to be 500 μm, 150 μm, 100 μm, ≤50 μm and ≤30 μm (fig.1). The Mg and B powders were thoroughly homogenized in agate mortar and then pelletized under the uniaxial hydraulic press. The prepared pellets were then taken in Fe tube closed at one end, which was in turn placed in the tube furnace for annealing. The annealing was performed at around 800°C for one hour under the continuous flow of 5N pure Ar gas to establish an inert environment. The synthesized samples were then subjected for X-ray diffraction using Rigaku D/Max 2200 Cu Kα radiations (1.54Å) to study its crystal structure. The precursor Mg powders along with the synthesized pellets were studied for their morphology by using HITACHI S-4700 FESEM. Superconducting transition in the sample was studied by measuring resistivity by collinear four probe technique as well as zero-field-cooled and field-cooled magnetization measurements using Quantum Design physical property measurement system model no. 6000. The magnetization hysteresis (M-H) measurements were carried out to determine irreversibility field. The critical current density was estimated by revoking the modified Bean's critical state model as shown in equation (1) below [10].

$$J_c = \frac{20\Delta M}{a\left(1-\frac{a}{3b}\right)} \quad (1)$$

Where, Jc is critical current density in A/cm^2, ΔM is the difference in the magnetization in emu/cm^3 for increasing and decreasing field, 'a' and 'b' is the thickness and width of sample.

3. RESULT AND DISCUSSIONS

In the present study Mg precursor with different particle size is reacted with boron. The particle size of Mg was estimated from SEM images as shown in Fig. 1(a)-(e).

* Corresponding author: kcchung@kims.re.kr

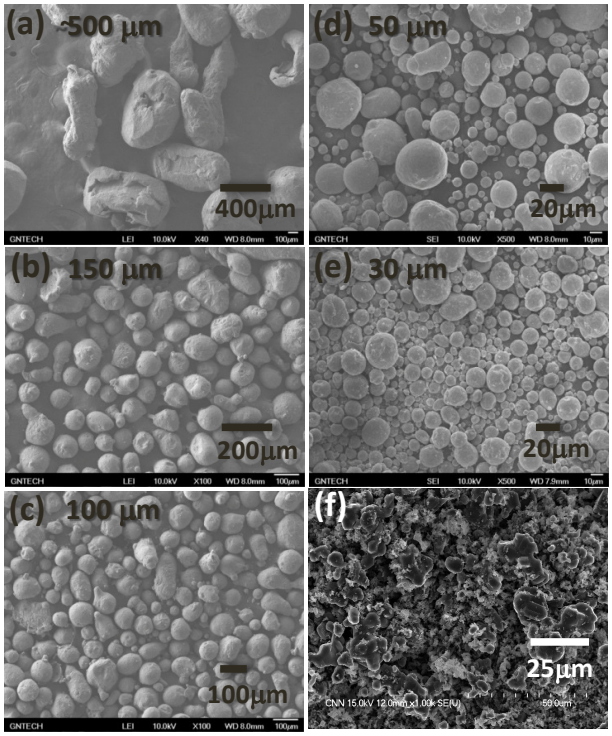

Fig. 1. FE-SEM images of Mg (a)-(e) and B (f) precursor powder.

Fig. 1(f) depicts the SEM image of boron precursor with the particle size of around 20 µm or less. From Fig. 1(a)-(e) it can be established that the largest particle size of Mg precursor is of 500 µm while the lowest particle size is around 30 µm. The Mg precursor powder corresponding to larger particle size (Fig. 1(a)-(c)) shows more or less uniform size distribution. This is not in case of Mg with smaller particle size (50 µm) Fig 1(d) and (30 µm) Fig 1(e) which shows widely varying particle size. In these two cases, we observe that the particle size is less than or equal to 50 µm or 30 µm and hence consider the same as the size label respectively. According to the particle size of Mg precursor, we designate the synthesized MgB_2 samples as BM500, BM150, BM100, BM50 and BM30.

3.1. X-ray diffraction studies

Fig.2 shows the X-ray diffraction pattern for the samples BM30 – BM500. These patterns depicts that MgB_2 forms the dominant phase in case of all the samples. All the peaks corresponding to MgB_2 are indexed as shown in fig.2. There appears to be a presence of MgO peak at around 62° which seems to be practically unavoidable considering the oxide impurity coming from precursors as well as processing conditions. The average volume percentage of MgO qualitatively determined from the XRD was found to be around 10% in all the samples.

No X-ray detectable impurities corresponding to other phases such as Mg-deficient compounds or unreacted boron etc. were found. Further there was a scarcely noticeable peak at around 36° of unreacted Mg, although, there can be traces of Mg present in the sample that are undetectable for X-rays.

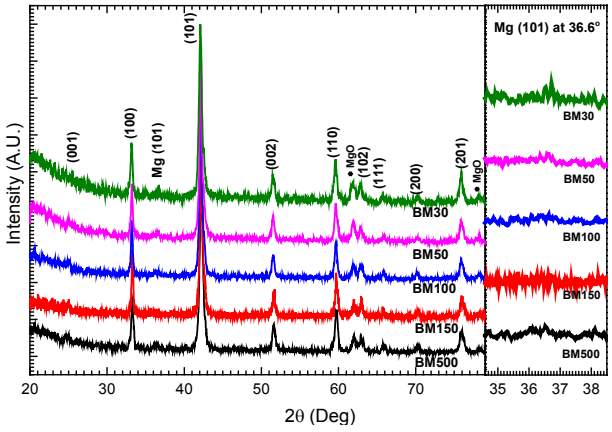

Fig. 2. X-ray diffraction patterns of the synthesized MgB_2 samples as the size of Mg precursor increases.

TABLE I
FWHM VALUES AND AVERAGE CRYSTALLITE SIZE CORRESPONDING TO SYNTHESIZED MGB_2 SAMPLES.

Samples	FWHM (Deg)					MgB_2 Average Crystallite size (nm)
	(1 0 0)	(0 1 0)	(0 0 2)	(1 1 0)	MgO	
BM500	0.35	0.51	0.44	0.47	0.54	20.0
BM150	0.28	0.43	0.43	0.42	0.58	22.9
BM100	0.28	0.44	0.41	0.41	0.56	23.2
BM50	0.28	0.45	0.41	0.48	0.58	22.3
BM30	0.34	0.51	0.49	0.49	0.65	19.5

Table 1 gives the values of FWHM for all the main peaks corresponding to MgB_2 and MgO phase along with the average crystallite size of MgB_2 as calculated by Scherrer's formula. It is understood that the crystallite size of MgB_2 is mainly influenced by size of boron particles rather than Mg since it is the boron particles that remains intact against Mg that melts and diffuses in boron. Accordingly, the crystallite size of MgB_2 remains more or less in the range of 19 to 23 nm and does not show considerable variation even though the size of Mg precursor is widely varied. The SEM image of B precursor in fig. 1(f) gives an idea of B particle size which varies within 30 µm, which gives justifies the size of MgB_2 crystallites. Nevertheless within this small range, crystallite size is lowest for BM 30, marginally increases with the size of Mg except for BM500 where it again decreases. The lattice parameter at the same time do not show any variation and was found to be a=3.08 Å and c=3.52 Å.

3.2. Cross sectional FE-SEM Morphology

The FE-SEM images of all samples along the fractured surface at two different magnifications are given in fig. 3. The morphology at low magnifications fig. 3 (a)-(e) makes some interesting revelations. It is observed that samples with large Mg particle size BM500 and BM150 incorporates large sized pores while sample with small particle size BM30 has smaller pores. Somehow no pores are observed for the samples with intermediate sized Mg particles. Although it seems hard to understand whether samples with large or small Mg particle size has more

number of pores. But it is evident that the samples BM500 and BM150 has pores that are quite elongated and deep while the same for BM30 are comparatively shallow and confined to small irregular ellipsoidal space. To understand this, we should consider the immediate reaction dynamics between Mg and B particles.

In MgB_2, the reaction progresses by the diffusion of liquid or gas phase Mg atoms into a rather intact boron lattice. This diffusion can be hindered only by the impurity or diffusion length or boron wetting by Mg. Since no dopant was added the question of extrinsic impurity can be ruled out while the intrinsic impurities can be considered to be uniform in all the samples. The second factor of diffusion length hence might play some role. In a well homogenized mixture of Mg and B, for larger Mg particle size, more Mg will be concentrated at a point as compared to smaller Mg particle size. This will naturally require the Mg concentrated at a localized point to travel a larger length to diffuse in to boron as compared to small sized Mg particle that will provide a better wetting of B as compared to large sized Mg particle [11]. Meanwhile, the tendency of Mg evaporation gives more chance for the creation of big pores in case of large sized Mg precursor. This probably explains the large elongated pores in sample BM500 and BM150 while small sized pores for sample BM30.

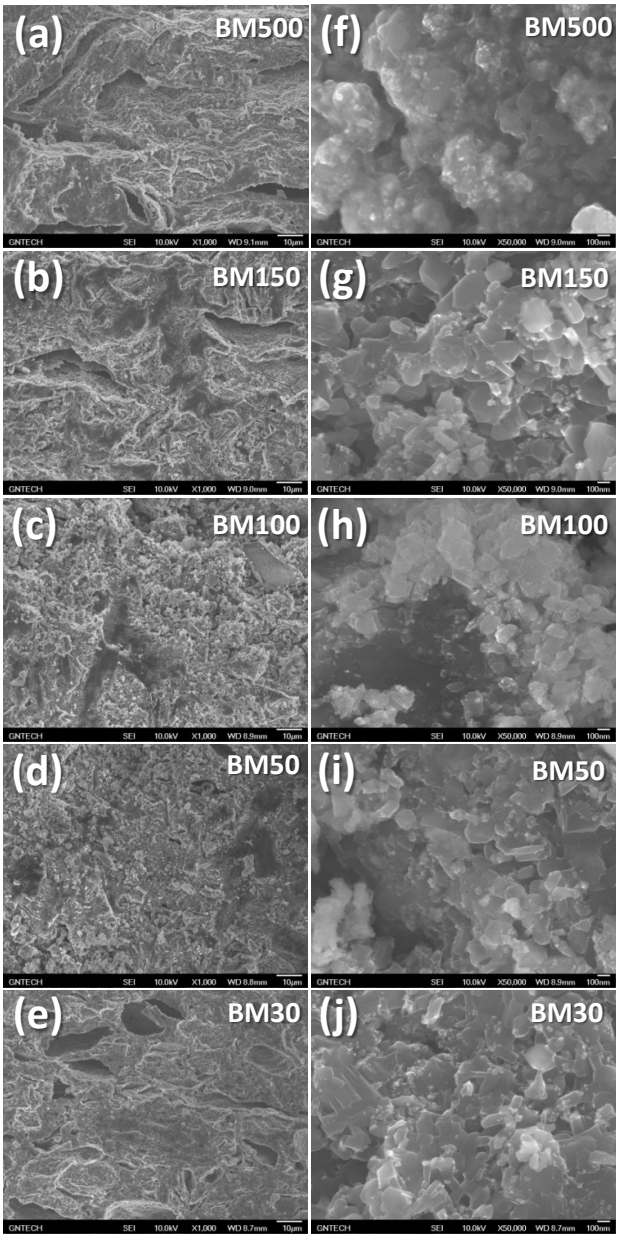

Fig. 3. FE-SEM images of the fractured surface of all samples with different magnificatinos of (a)-(e) X1000 and (f)-(j) X50000.

The high magnification images fig.3.(f)-(j) shows the typical grain structure of MgB_2. Further, the better wetting of B by Mg of smaller size will naturally give a comparatively good grain homogeneity and grain to grain connectivity than the large size of Mg. This is inevitably depicted in the high magnification images for all the samples. Rather fused grain morphology for (fig.3. (f)) BM500 along with the presence of large pore like opening again stresses upon the effects of larger Mg particle size of precursor. Since there was no evidence of any significant peak of Mg in the XRD for BM500, the presence of excessive metallic Mg can be negated, which can be explained by the possibility of quick evaporation of liquid Mg [12] during the reaction leaving behind pore like openings. Nevertheless the possibility of XRD-blind Mg traces cannot be completely ruled out. Moreover, considering the large size of Mg precursor (about 500 μm) the fused grain like morphology as against other samples refers to the incomplete recovery and recrystallization process.

3.3. Superconducting transition

Fig.4 shows the normalized resistivity plots three representative samples BM500, BM100 and BM30 corresponding to the highest, intermediate and lowest particle size of Mg precursor. The data is in concurrence with the reported results [12] for the MgB_2 bulk samples that are prepared by varying Mg:B ratio. The sample with larger Mg precursor size has more temperature dependence of resistivity as compared to the sample with smaller Mg precursor size. This can be probably due to presence of Mg at the grain boundaries which has influenced the resistivity behavior. This is in line with the discussion made on morphological analysis, that large sized Mg precursor will contribute towards slower overall diffusion process intending to leave traces of Mg along the grain boundary, that in-turn contributes towards a greater temperature dependence of resistivity [12].

This is not in case of samples involving precursor with smaller Mg particle size. Better diffusion in B reduces the presence of metallic Mg along the grain boundary thereby helps in achieving better grain to grain contact that relatively decreases the slope of resistivity curve. The superconducting transition for all the samples remains more or less constant at around 36 K irrespective of Mg precursor size.

The superconducting transition was further confirmed by the Zero-field-cooled (ZFC) measurement on all the samples in the series. All the samples have shown around same diamagnetic transition temperature of 36.0 K that is in agreement with the resistivity measurements.

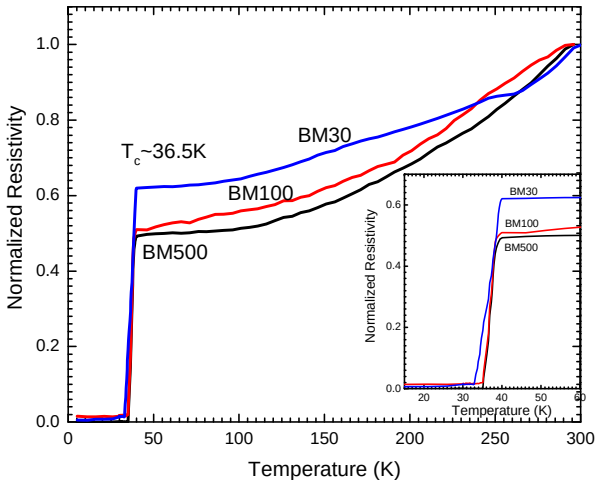

Fig. 4. Normalized resistivity versus temperature curves for samples BM500, BM100 and BM30.

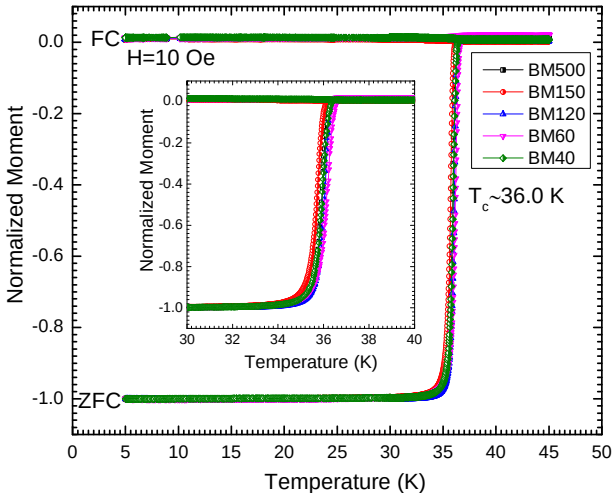

Fig. 5. Normalized magnetization versus temperature plots for all samples.

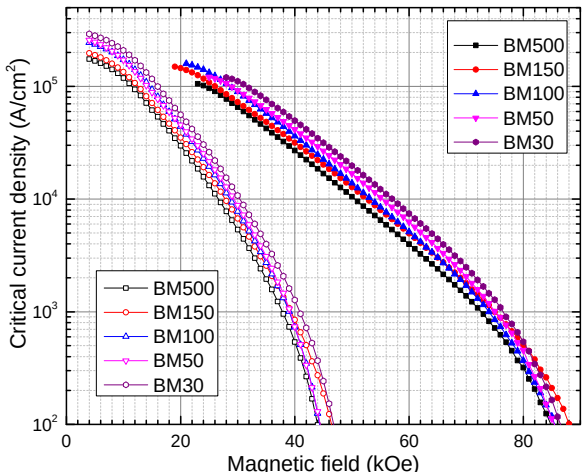

Fig. 6 The critical current density versus magnetic field plots at 5K and 20K for all samples.

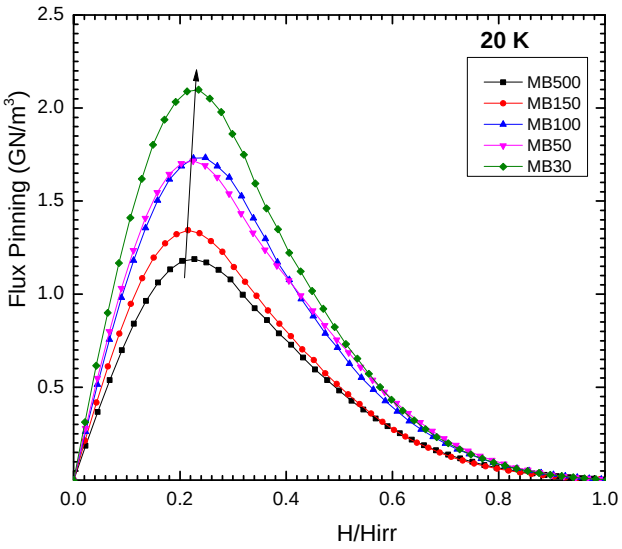

Fig. 7. Flux pinning plots for all the samples at 20K.

3.4. Critical current density

Fig.6 shows the critical current density, which were obtained by applying Bean's model, versus magnetic field curves at 5K and 20K for all samples. All samples were maintained in same size with thickness, width and length being 1 mm, 2 mm and 3 mm respectively. It can be seen from fig. 6 that the overall critical current density value for the sample BM30 is higher while the same for BM500 is lower than all other samples. The low field critical current density values for all the samples decreases with the increase of the Mg precursor particle size. It is well known that at low field critical current density values are directly related to the grain-to-grain connectivity [13]. Thus higher critical current density value for sample BM30 and subsequent decrease for rest of the samples along with successive increase in Mg precursor particle size is well in support to our previous argument of better grain connectivity.

3.5. Flux pinning studies

The flux pinning force was calculated using relation $F_p = J_c \times \mu_o H$ [14]. The MgB_2 samples are considered to be grain boundary pinned provided there are no artificially introduced pinning centers. From fig. 7, the flux pinning force for sample BM30 is observed to be much greater than all other samples. Further the peak position of the flux pinning curves show a slight but gradual shift towards higher values of the field for the samples from BM500 to BM30. Thus, it can be understood that the smaller sized Mg precursor leads to increased flux pinning force. This might be the combined effect of relatively smaller grain size of MgB_2 and inclusion of small quantity of MgO impurity that can infiltrate in the samples by the virtue of greater surface area of Mg particles with smaller size.

4. CONCLUSIONS

The influence of Mg precursor size on the MgB_2 samples synthesized by solid state synthesis route was studied. It

was found that the large sized Mg precursor (500 μm) resulted in to incomplete recovery and recrystallization process. Presence of unreacted metallic Mg was expected at the grain boundary for the samples synthesized with higher Mg precursor size. This resulted in greater dependence of resistivity on temperature even though the transition temperature remained same at around 36 K. As the Mg precursor size is decreased, better grain connectivity with smaller pores was obtained that resulted in the overall increase in the critical current density of the sample.

ACKNOWLEDGMENT

This work was supported by the Global Research Laboratory Program through a grant funded by the National Research Foundation of Korea (2012-00184).

REFERENCES

[1] J. Nagamatsu, N. Nakagawa, T. Muranaka, Y. Zenitani, and J. Akimitsu, "Superconductivity at 39K in magnesium diboride," *Nature*, vol. 410, pp. 63, 2001.

[2] Y. Bugoslavsky, L. F. Cohen, G. K. Perkins, M. Polichetti, T. J. Tate, R. Gwilliam, and A. D. Caplin, "Enhancement of the high magnetic field critical current density of superconducting MgB_2 by proton irradiation," *Nature (London)*, vol. 411, pp. 561, 2001.

[3] D. C. Larbalestier, L. D. Cooley, M. O. Rikel, A. A. Polyanskii, J. Jiang, S. Patnaik, X. Y. Cai, D. M. Feldmann, A. Gurevich, and A. A. Squitieri, "Strongly linked current flow in polycrystalline forms of the superconductor MgB_2," *Nature (London)*, vol. 410, pp. 186, 2001

[4] T. C. Shields, K. Kawano, D. Holdom, and J. S. Abell, "Microstructure and superconducting properties of hot isostatically pressed MgB_2," *Supercond. Sci. Technol.*, vol. 15, pp. 202, 2002.

[5] S. X. Dou, S. Soltanian, J. Horvat, X. L. Wang, S. H. Zhou, M. Ionescu, H. K. Liu, P. Munroe, and M. Tomsic, "Enhancement of the critical current density and flux pinning of MgB2 superconductor by nanoparticle SiC doping," *Appl. Phys. Lett.*, vol. 81, pp. 3419, 2002

[6] J. Wang, Y. Bugoslavsky, A. Berenov, L. Cowey, A. D. Caplin, L. F. Cohen, J. L. MacManus Driscoll, L. D. Cooley, X. Song, and D. C. Larbalestier, "High critical current density and improved irreversibility field in bulk MgB2 made by a scaleable, nanoparticle addition route," *Appl. Phys. Lett.*, vol. 81, pp. 2026, 2002

[7] H. Kumakura, H. Kitaguchi, A. Matsumoto, and H. Hatakeyama, "Upper critical fields of powder-in-tube-processed MgB2/Fe tape conductors," *Appl. Phys. Lett.*, vol. 84, pp. 3669, 2002.

[8] Y. Bugoslavsky, L. F. Cohen, G. K. Perkins, M. Polichetti, T. J. Tate, R. Gwilliam, and A. D. Caplin, "Enhancement of the high magnetic field critical current density of superconducting MgB_2 by proton irradiation," *Nature (London)*, vol. 411, pp. 561, 2001

[9] S. G. Jung, W. K. Seong and W. N. Kang, "Effect of columnar grain boundaries on flux pinning in MgB_2 films," *J. Appl. Phys.*, vol. 111, pp. 053906, 2012.

[10] A. Serquis, X. Z. Liao, Y. T. Zhu, J. Y. Coulter, J. Y. Huang, J. O. Wills, D. E. Peterson, F. M. Mueller, N. O. Moreno, J. D. Thompson, V. F. Nesterenko and S. S. Indrakanti, "influence of microstructures and crystalline difects on the superconductivity of MgB_2," *J. Appl. Phys.*, vol. 92, pp. 351, 2002.

[11] D. Wang, Y. Ma, Z. Yu, Z. Gao, X. Zhang, K. Wantanabe and E. Mossang, "Strong influence of precursor powder on the critical current density of Fe-Sheathed MgB_2 tapes," *Supercond. Sci. Technol.,* vol. 20, pp. 574, (2007).

[12] S. K. Chen, A. Serquis, G. Serrano, K. A. Yates, M. G. Balmire, D. Guthrie, J. Cooper, H. Wang, S. margadonna and J. L. McaManus-Driscoll, "Structural and superconducting property variations with nominal Mg non-stoichiometry in Mg_xB_2 and its enhancement of upper critical field," *Adv. Funct. Mater.*, vol. 18, pp. 113, 2008.

[13] M. Maeda, J.H. Kim, S. Oh, W.X. Li, K. Takase, Y. kuroiwa, S.X. Dou and Y. Takano, "Enhancing the superconducting properties of magnesium diboride without doping," *J.Am. Ceram. Soc.,* 12419, pp. 1-5, 2013.

[14] B.B. Sinha, M.B. Kadam, M. Mudgel, V.P.S. Awana, H. Kishan and S.H. Pawar, "Synthesis and characterization of excess magnesium MgB_2 superconductor under inert carbon environment," *Physica C,* vol. 470, pp. 25-30, 2010.